Genetically aerodynamic optimization of the nose shape of a high-speed train entering a tunnel

J. Muñoz-Paniagua *, J. García, A. Crespo

Grupo de Investigación de Mecánica de Fluidos aplicada a la Ingeniería Industrial, Escuela Técnica Superior de Ingenieros Industriales, Universidad Politécnica de Madrid, C/ José Gutiérrez Abascal 2, 28006 Madrid, Spain

A B S T R A C T

The optimization of the nose shape of a high-speed train entering a tunnel has been performed using genetic algorithms (GA). This optimization method requires the parameterization of each optimal candidate as a design vector. The geometrical parameterization of the nose has been defined using three design variables that include the most characteristic geometrical factors affecting the compression wave generated at the entry of the train and the aerodynamic drag of the train. A large set of three-dimensional, turbulent, compressible, unsteady simulations of realistic train models have been done, and this information has been used to fit a metamodel. The metamodel is used by the GA to evaluate each optimal candidate in a more efficient way. The optimal designs that minimize the maximum pressure gradient and the aerodynamic drag are in good agreement with the literature. To complete this single-objective optimization, a multi-objective optimization has been developed, and a Pareto front has been obtained. The use of metamodels has permitted to analyze the influence of each design variable.

Keywords:
High-speed train
Tunnel
Shape optimization
Genetic algorithm
Aerodynamic drag
Maximum pressure gradient

1. Introduction

The requirements for an efficient mean of transportation are met in high-speed trains, what make them interesting enough to attract much attention from researchers to develop lighter and faster trains. A consequence of this evolution is the introduction of new problems that were neglected before but are notably significant nowadays. Thus, the aerodynamic optimization plays a key role in the design process of a high-speed train. This aerodynamic optimization becomes into a multi-objective optimization, as many different problems may be considered, and some of them are known to be in conflict (Krajnovic, 2009). These aerodynamic problems are even more intense when the train travels at high speed through a gallery like a tunnel (Howe et al., 2000). The presence of tunnels is unavoidable in railways, and actually many reasons let us conclude that there will be even more (Heine and Ehrenfried, 2012). Consequently, the aerodynamic optimization involving high-speed trains running through a tunnel is of major interest.

The aerodynamic consequences of high-speed trains running in a tunnel are basically resumed in two correlated phenomena, the generation of pressure waves and an increase in aerodynamic drag (Schetz, 2001). The most relevant factors affecting the pressure waves nature and the aerodynamic drag are the train geometry, the operating conditions and the tunnel design. The latter has been the subject of numerous investigations, considering the entrance and exit (Auvity et al., 2001, Howe et al., 2000, Yoon et al., 2001), or airshaft apertures on the tunnel surface (Howe, 2005, Vardy, 2008 or Yoon et al., 2001). The influence of the tunnel design on the aerodynamic drag is considered in Baron et al. (2001) or Gawthorpe et al. (1979). The effect of the nose length has been studied by Auvity et al. (2002), Baron et al. (2006), Bellenoue et al. (2002), Matsuo et al. (1997) or Vardy (1996), while an analysis of the influence of the nose shape is presented in Iida et al. (1996), Ku et al. (2010) or Kwon et al. (2001). Other factors, as the train position with respect to the tunnel axis, the track form and the train speed are analyzed in Ogawa and Fujii (1997), N'Kaoua et al. (2006) or Baron et al. (2006).

The optimization of aerodynamic properties of high-speed trains has traditionally been handled as a trial-and-error procedure, which relies on engineers experience. New computational methods and the increase of the computational power permit nowadays new optimization methods to be applied. The application of these methods is very popular in aircraft or vehicle aerodynamics, but is still in progress in train aerodynamics. The tunnel entrance has been genetically optimized in Howe (2007) using genetic algorithms (GA). Considering the nose shape, Krajnovic (2009), Vytla (2011) or Jakubek and Wagner (2012) resolve different optimization problems in open air using either GA or adjoint methods. In the case of trains in

* Corresponding author.
E-mail address: le.munoz@upm.es (J. Muñoz-Paniagua).

tunnels, the optimization of the nose shape using new optimization methods is accomplished in Lee and Kim (2008) or Kwon et al. (2001). Kikuchi et al. (2011) use GA for the train nose shape optimization in combination with a calculation program called BUHOOD (Howe et al., 2006), based on acoustic theory. This program takes into account the tunnel entrance hoods and permits to rapidly calculate the compression wave generated by the train entering a tunnel. In most of the previous references, the train model used is an axially symmetric model instead of a more realistic three-dimensional (3D) train model. In that case, the shape optimization consists in determining the optimal cross-section profile of a train by means of axially symmetrical models, and then transforming it into a three-dimensional train model that retains the same area space evolution.

1.1. The scope of the study

These observations, the former parametric studies and the increasing importance of new optimization methods let us propose the following points.

- One step forward is to directly consider realistic geometries instead of axially symmetrical models. The first objective is to run a set of three-dimensional, turbulent, compressible, unsteady simulations to investigate the effect of three design variables (nose length, nose shape and blockage ratio) on the maximum pressure gradient and the aerodynamic drag on the train.
- GA are not exactly novel, but the application of them in the aerodynamic optimization of high-speed trains is relatively new. We use GA to optimize the nose shape of a high-speed train entering a tunnel. This method has been used in this scenario, but considering analytical methods based on an acoustic theory. To our knowledge, our paper is the first application of GA and numerical simulation methods (CFD) for the shape optimization of high-speed trains in tunnels. A description of the method, its requirements and capabilities are included.
- Kikuchi et al. (2011) suggest that CFD is not suitable for the design process because the GA requires a large number of solver calls. In this paper, the use of surrogate models or metamodels is presented as an alternative to reduce the number of solver calls and thus CFD can be considered instead of analytical methods for the evaluation of each optimal candidate.
- The third objective is to take advantage of all the information used for and contained in the metamodel required by the GA to yield insight into the design space nature. An analysis of variance (ANOVA) test completes it. These results let us obtain a relationship between the maximum pressure gradient, the pressure amplitude and the design variables. This task was pointed out to need further investigation in Bellenoue et al. (2002), but there is not yet too much information about it.
- To conclude the study, we solve the multi-objective optimization problem, considering as the objective functions the maximum pressure gradient and the drag coefficient. We obtain a Pareto front that contains a set of optimal solutions, where the best designs for each single objective are included as well.

The paper is organized as follows. In Section 2 the methodology used for solving the optimization problem is described. This encompasses the GA work-flow and the numerical set-up. The discussion of the results, a parametric study of the influence of the design variables and the information of the metamodel are presented in Section 3. The conclusions of the multi-objective optimization are introduced in Section 4. Finally, Section 5 is devoted to the summary.

2. Methodology

The optimization method selected to solve this multi-objective problem is the genetic algorithms (GA). GA, introduced by Holland (1975) and developed by Goldberg (1989), are a technique that mimic the mechanics of the natural evolution. Once a population of potential solutions is defined, three operators (selection of the fittest, reproduction or crossover and mutation) are applied, Fig. 1. Iteratively, a new population is generated and better results are obtained until a solution closer to globally optimal solution is reached. The combination of the survival-of-the-fittest concept to eliminate unfit characteristics with a random information exchange and the exploitation of the knowledge contained in old solutions

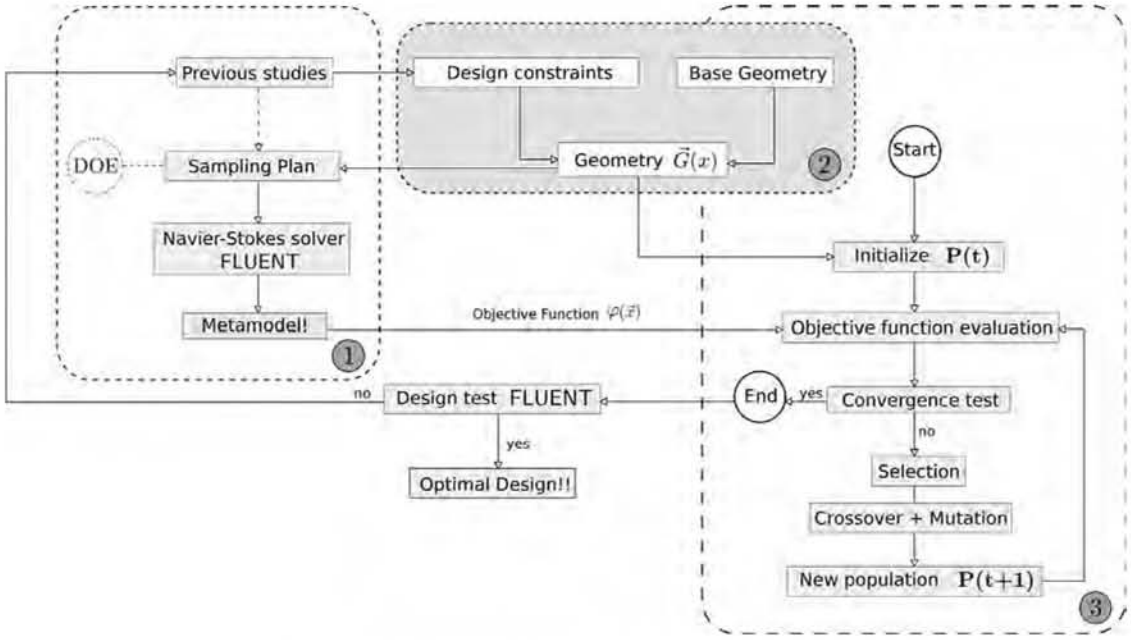

Fig. 1. Schematic representation of the whole optimization scheme.

permit GA to effect a search mechanism with efficiency and speed. GA are englobed in zero-order methods, based on direct evaluations of the objective function. This is an advantage compared to first-order methods that need the calculation of the first derivative of the objective function. However, the large number of evaluations required when using GA is a disadvantage that minimizes its power. Furthermore, this behavior is emphasized in this case, where the nature of the aerodynamics of the train/tunnel system (three-dimensional, turbulent, unsteady, compressible flow) implies an additional computational cost.

To minimize the problem of the large number of evaluations required by the GA, which directly depends on the dimensionality of the design space, a very simple geometric parameterization was proposed. Additionally, the CFD solver call was substituted by a metamodel. The present increase of the computational power is not sufficient to conceive a thorough search of the design space using accurate simulations. This situation, which is stressed in this scenario, leads to the introduction of an approximate model whose computational cost is much lower than the relative to the CFD simulation. In Fig. 1, a very conventional optimization work-flow is represented. This scheme refers to an online optimization, where after the end of the GA optimization process, the best solution found by the surrogate-based optimizer is evaluated and verified, and this new simulation is added to the initial database that was used to train or fit the coefficients of the metamodel.

2.1. Geometric parameterization

Any optimal candidate needs to be represented by a set of design variables or parameters. The proposed geometric parameterization has to be simple enough to make this optimization study affordable in terms of computational cost. The parameterization here presented is based on a baseline geometry. This reference geometry is called 'generic train' (Sima et al., 2011). From it, one extra design variable is introduced here to give more diversity to the design space and capture the nose bluntness effect. Any optimal candidate is defined in terms of three design variables, $\{l_1, l_2, R_1\}$. The nose length l_1 controls the shrinking of the nose and, following the Raghunathan proposal (Raghunathan et al., 2002), l_1 varies from $[w, 4w]$, where w is the train width. Length L given in Fig. 2 refers to the total length of the train head, which is kept constant ($L=15$ m). The length l_2 refers to the bluntness of the nose (top view), and its range of variation is $[\frac{1}{6}w, \frac{1}{3}w]$. Finally, radius R_1 defines the A-pillar roundness and let us change the cross-sectional area of the train and the bluntness of the nose tip. R_1 varies from $[\frac{1}{6}w, \frac{1}{4}w]$. This parameterization is sketched in Fig. 2. Geometries are parametrically defined in CATIA®. Height H and width w are set constant for all the geometries. H is 3.850 m and w is 3.000 m. Nose tip height and tip roundness are also the same for all the cases, with $r_t=0.750$ m. Clearance c between the top of the rail and the bottom of the train is set to 0.250 m. The radius that controls the connection between the nose and the rest of the car is $r_c=0.750$ m.

2.2. Metamodel definition

It has been indicated that the main drawback of the GA is the large number of evaluations required by the optimization method to find an optimal design. Each evaluation is usually a solver call, and the number of solver calls depends on the population size and the number of generations necessary to obtain the optimal design. This number of solver calls can be dramatically reduced if approximation models or metamodels are used with the GA. This is referred as surrogate-based optimization.

This number of evaluations is a function of the number of individuals in the population and the number of generations necessary to obtain such optimal design. Apart from simplifying the geometric parameterization, the use of metamodels or approximation models permits the GA process to be speed up since, by using approximation models, the expensive simulation model is replaced. The metamodel technique chosen in this paper is the radial basis function (RBF). It uses a linear combination of m radial basis functions

$$\hat{y}(\mathbf{x}) = \sum_{i=1}^{m} \omega_i \phi(|\mathbf{x}-\mathbf{x}_i|) \tag{1}$$

to approximate the response $y(\mathbf{x})$. $\phi(d_i)$ is called the radial basis function, such that the radial distance d_i is defined as $d_i = |\mathbf{x}-\mathbf{x}_i|$ centered at the point $\mathbf{x}_i$. The norm $\|$ is the Euclidean distance. w_i is the weight of radial basis function i in the linear combination aforementioned. The radial function used here is the Gaussian function:

$$\phi(d_i) = \exp\left(-\frac{d_i^2}{2|\mathbf{r}_i|^2}\right) = \exp\left(-\frac{|\mathbf{x}-\mathbf{x}_i|^2}{2|\mathbf{r}_i|^2}\right). \tag{2}$$

The construction of the RBF networks demands the estimation of some parameters. Apart from setting the weights in Eq. (1), the number of hidden units m, the spread $\mathbf{r}_i$ and the centers $\mathbf{x}_i$ are the

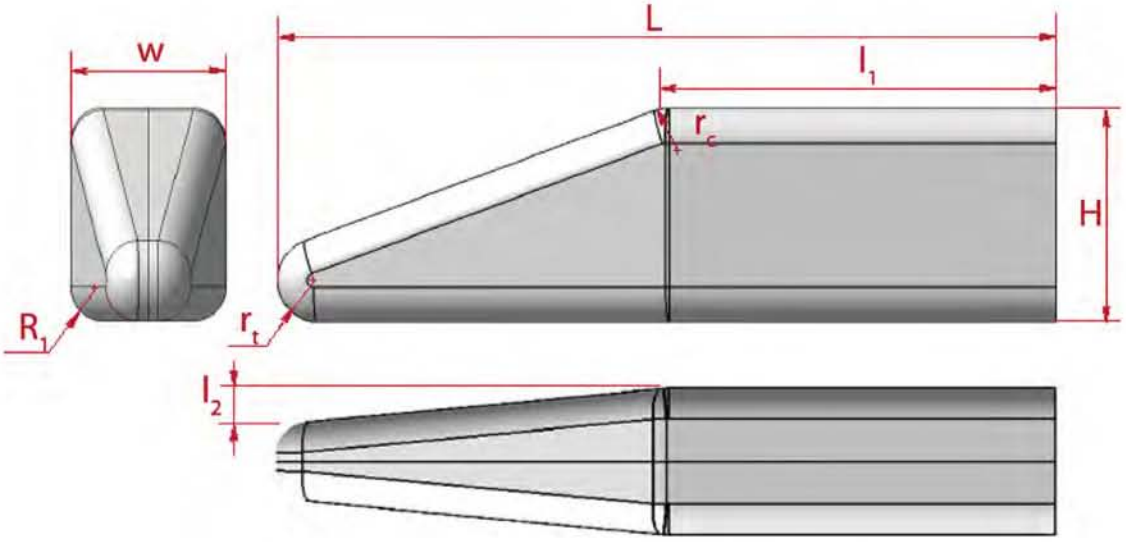

Fig. 2. Geometric parameterization used to define the optimal candidates.

other parameters to be defined. The number of neurons m is set equal to the size of the design of experiments N (Section 2.3), and the centers do coincide with the sampling points. The spread is fixed for all basis functions but varies for each design variable. The initial value is first estimated by the relation $r = d_{max}/\sqrt{m}$, where d_{max} is the maximum distance between any two centers. Ridge regression (Orr, 1996) is used to control the model sensitivity (avoid the model to overfit the data and to mislead variations due to imprecise or noisy data). A regularization parameter λ is introduced to the sum-squared-error expression applied to determine the optimal weight vector $\{\omega\}_{i=1}^{m}$. Orr proposes a parametric study to find the parameter λ and this strategy is also used in this paper. The model selection criteria used to find λ (and r) is the generalized cross-validation (GCV).

2.3. Initial design of experiments

The metamodel is constructed with a sampling plan of the design space. This sampling plan is called design of experiments (DoE) and will be used to fit the parameters of the metamodel. A three-dimensional 'maximin' Latin Hypercube design (LHD) of fifteen points ($N=5n$, where n is the dimensionality of the design space) is used to generate the DoE. A database of the best designs of LHD is included in Husslage et al. (2006), from where the design used here is obtained. The resulting DoE is detailed afterwards.

2.4. Numerical set-up

The computational domain is composed of the tunnel and the tunnel entrance. To avoid the interaction of the entry compression waves and the reflected waves at the exit of the tunnel, the end of the tunnel is not included in the computation. This situation is known as infinite length tunnel. The tunnel is 300 m long, which is enough to permit an investigation of the transient flow at the tunnel entry (Ogawa and Fujii, 1997). In order to not consider the effect of the tail entering the tunnel, an infinite length train is modeled (200 m). The surroundings of the entrance of the tunnel are dimensioned so that the domain boundaries do not affect the flow close to the tunnel portal. The boundaries are 30 m far from the longitudinal symmetry axis of the train. At the beginning of the computation, the train is placed far from the tunnel entrance, so that the numerical simulation can be stabilized. An intermediate zone of 150 m long is considered upstream the train nose, as it is indicated in Fig. 3. The tunnel cross-sectional area is $A_T=63$ m^2. The railway is simple-tracked, so the train body is placed at the center of the tunnel section. The blockage ratio, depending on which is the exact cross-sectional area of the train for each design, varies between 0.176 and 0.180. The actual values are given in the next sections.

The train speed is 250 km h^{-1}, meaning a Mach number of $M=0.2$. A compressible, unsteady, turbulent flow simulation is considered. Simulations are run using ANSYS – FLUENT® CFD software. The standard k–ϵ turbulence model is used, with second order upwind momentum and time discretization scheme. The simulation of a train moving in a gallery involves the relative motion of the train with respect to the tunnel walls. This motion is modeled using the sliding mesh technique. A grid-independence analysis was performed, varying the distance of the closest point to the train surface y, the resolution of the mesh in the streamwise direction Δx^+ and the timestep. The total number of cells is $\sim 6\times10^6$. All the cells are hexahedral. The time step Δt is 0.001 s, which is sufficiently small to resolve the unsteadiness in the flow field. The boundary layer is captured all along the train surface and the ground, but not in the tunnel walls. The standard wall functions implemented in the CFD software are used, and $y^+ = u_\tau y/\nu$, where u_τ is the wall friction velocity and ν is the kinematic viscosity of air ($\nu=1.45\times10^{-5}$ m^2 s^{-1}), is fixed to 100. Δx^+ in terms of wall units y^+ is 25–250. The boundary conditions are indicated in Fig. 3.

3. Discussion of the results

3.1. Initial design of experiments

The first fifteen simulations run to train the metamodel yield insight into design variables effect on both the drag coefficient and the maximum pressure gradient. Information about these magnitudes, and also the pressure rise and the main geometric characteristics of each design point are given in Table 1. The aerodynamic drag is computed for this infinite length train restricting its value to the train head (see Fig. 2) and a section of the train body of length 35 m. Graphics of the pressure rise and the corresponding pressure gradient are not included in this section but the most representative cases are plotted in the Section 3.2, including the optimum solutions. Our results are in good agreement with those presented in Sima et al. (2011) for a generic train model. The pressure rise can be calculated using the equation given in Miyachi et al. (2012), which introduces the equation of Hara (1961) to predict the pressure rise of the compression wave in a new easy way. Our values differ from these in less than a 4%, what validates our computations

$$\Delta p \approx \frac{1}{2}\rho U^2 \frac{1-(1-R)^2}{(1-M)((1-R)^2+M)} \tag{3}$$

where $\phi = 1-\beta = 1-A_c/A_T$, being A_c the cross-sectional area of the train. It is observed that the nose length has a critical impact on the maximum pressure gradient, while the pressure rise and the drag coefficient are more related to the cross-sectional area and the bluntness of the nose. A larger nose (lower value of l_1) gives a lower

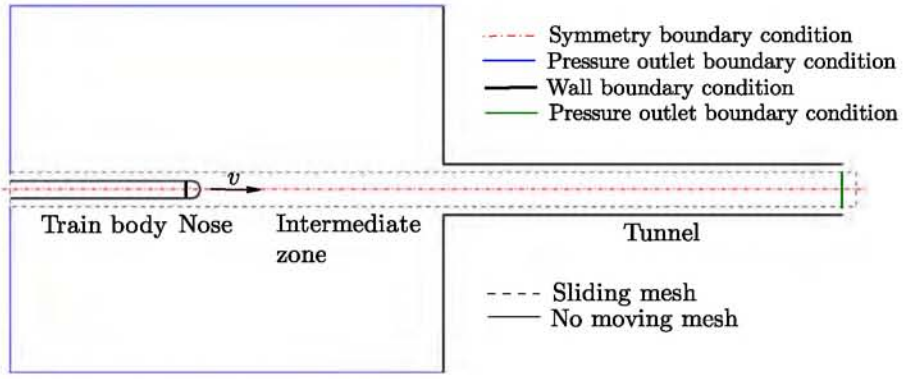

Fig. 3. Description of the flow domain and the boundary conditions for the numerical simulations.

Table 1
Design variable values and geometrical characteristics of the geometries included in the initial design of space. A_c refers to the train cross-sectional area, while β is the blockage ratio. The coefficient k is defined in Section 3.6.

Geo #	l_1 (m)	l_2 (m)	R_1 (m)	A_c (m^2)	β	C_D	$\frac{\partial p}{\partial t}$ (Pa s^{-1})	Δp (Pa)	k
1	3.000	0.679	0.607	11.195	0.178	0.127	5502.0	1347.7	0.586
2	3.643	0.929	0.571	11.270	0.179	0.133	5931.7	1360.8	0.548
3	4.286	0.643	0.732	11.090	0.176	0.125	5767.8	1329.3	0.552
4	4.929	0.893	0.696	11.134	0.177	0.119	6143.2	1332.0	0.521
5	5.571	0.536	0.536	11.304	0.179	0.141	6249.7	1372.4	0.522
6	6.214	0.786	0.500	11.335	0.180	0.133	6483.6	1370.9	0.505
7	6.857	0.500	0.661	11.175	0.177	0.148	6642.2	1357.7	0.484
8	7.500	0.750	0.625	11.215	0.178	0.138	6698.6	1334.2	0.482
9	8.143	1.000	0.589	11.252	0.179	0.137	6905.0	1313.1	0.470
10	8.786	0.714	0.750	11.067	0.176	0.145	7130.8	1340.6	0.445
11	9.429	0.964	0.714	11.112	0.176	0.157	7502.0	1358.3	0.425
12	10.071	0.607	0.554	11.287	0.179	0.165	7252.6	1333.8	0.449
13	10.714	0.857	0.518	11.320	0.180	0.182	7905.2	1408.1	0.413
14	11.357	0.571	0.678	11.155	0.177	0.170	7471.8	1349.9	0.429
15	12.000	0.821	0.643	11.195	0.178	0.184	7599.4	1337.5	0.424

maximum $\partial p/\partial t$. However, there are cases where shorter noses present a lower maximum peak if a proper combination of the other two design variables is given. This is put in evidence when comparing geometries #2 and #3. The latter is shorter, but is blunter, with a lower value of l_2. The cross-sectional area is also lower (larger R_1). Which of the two geometrical conditions affects more is not clear, but if geometries #11 and #12 are also analyzed, it is pointed out that the effect of a lower cross-sectional area is less important than the bluntness of the nose. However, these last two geometries have a very short nose length, with an slenderness ratio $s=2(L-l_1)/w$ lower than 2. Kwon et al. (2001) or Maeda et al. (1993) indicate that the effects of the shape optimization vanish for a slenderness ratio lower than this value, so it is not evident which effect is more important. The reason for this might be the fact that the flow is detached strongly in the case of a short nose, whereas it does not happen when the nose length is large. A strong flow detachment increases the blockage ratio so it might buffer the influence of the cross-sectional area.

Differences in the cross-sectional area of the train are evidenced in the different pressure rises, but these differences are negligible as it was expected from the blockage ratio range. Eq. (3) directly relates the pressure rise Δp caused by the compression wave at the entry of the train and the train cross-sectional area. However, from the results included in Table 1, it is observed that they do not exactly follow the tendency imposed in Eq. (3), as the smallest area (*i.e.* smallest blockage ratio) does not correspond to the smallest pressure rise. Our Δp was obtained by the difference of the mean values of the pressure between the intervals $\Delta t_1=(-0.4,-0.2)$ s and $\Delta t_2=(0.4,0.6)$ s, where $t=0.0$ s refers to the instant at which the nose tip enters the tunnel. Data is collected at $x=$ 50 m inside the tunnel, where $x=0$ m is the tunnel entry, $y=-0.5$ m from the longitudinal symmetry plane and $z=1$ m from the ground. It is concluded that the blockage ratio is not the only geometrical parameter to affect the pressure rise, but the nose shape, in particular the bluntness.

Drag coefficient is related both with the cross-sectional area and the bluntness of the nose. It is obvious that a larger cross-sectional area provokes a larger drag force, but also the shape of the nose does have a crucial impact on the aerodynamic drag. As it was expected, a larger value of l_2, which is translated into a sharper nose, leads to a reduction of the drag coefficient. The influence of the nose length on the drag coefficient is not so relevant as it was for the maximum pressure gradient.

The conclusions about the bluntness effect on the $\partial p/\partial t_{max}$ and the aerodynamic drag are also in good agreement with Iida et al. (1996), Lee and Kim (2008) or Ku et al. (2010). They reported that the micro-pressure wave at the tunnel exit (in other words, $\partial p/\partial t_{max}$) was weakened and the aerodynamic drag was increased as the front nose shape became blunt as it has been presented.

3.2. Minimization of the maximum pressure gradient

Before dealing with the multi-objective problem, a single-objective optimization problem is defined in first term. The minimization of the maximum pressure gradient is the objective function and, as it was indicated, a GA is used as the optimization method. The optimization process is run in MATLAB®, using the toolbox `globalOptimization`, included in the software. A surrogate-based online optimization problem is considered, letting the GA to use a metamodel to evaluate the fitness of the optimal candidates. The previous results are used to fit the metamodel. One of the advantages of using a RBF as the metamodel technique is that it is trained independently of the number of design variables and so the size of the initial design of experiments. Therefore, the fifteen cases were considered enough to construct the first metamodel. The training consists in determining the value of the spread and the regularization parameter, as it was indicated in Section 2.2. The spread r was defined individually for each design variable, because the effect of each one on the objective function is not the same. The resulting values were $r_i=(3.6,1.0,0.6)$. The regularization parameter was set to $\lambda=6.7\times10^{-5}$. An estimation of the prediction error is given by generalized cross-validation (GCV), whose final value is 3.1×10^{-3}.

After constructing the metamodel, a parametric study is required to fit the GA parameters. These parameters are the cross-over probability, the mutation probability, the population size, the selection function or the elitism size among others. In particular, two parameters were varied to determine the best performance of the GA. The best combination of the cross-over probability and the population size is selected regarding the optimal design found by the algorithm. The cross-over probability was finally set to 0.8, and the population size was set to 75. The

Table 2
GA parameters values.

Population size	75
Elitism	Yes
# elite individuals	2
Selection function	Tournament (2)
Scaling function	Ranking
Crossover function	Two-points
P_c	0.8
Mutation function	Uniform
P_m	0.01
# max generations	300

Table 3
Design variable values and geometrical characteristics of the geometries obtained during the optimization process. A_c refers to the train cross-sectional area, while β is the blockage ratio. The coefficient k is defined in Section 3.6.

Geo #	l_1 (m)	l_2 (m)	R_1 (m)	A_c (m^2)	β	C_D	$\frac{\partial p}{\partial t}$ (Pa s^{-1})	Δp (Pa)	k
1	3.000	0.679	0.607	11.195	0.178	0.127	5502.0	1360.8	0.586
o1	3.000	0.500	0.500	11.335	0.180	0.154	5572.0	1412.7	0.587
o2	3.000	1.000	0.750	11.067	0.176	0.116	5653.9	1290.3	0.602
o3	3.000	0.660	0.750	11.067	0.176	0.135	5449.7	1341.4	0.562
Optimal	3.000	0.500	0.750	11.067	0.176	0.144	5276.9	1343.1	0.583

other parameters were fixed. The corresponding values are summarized in Table 2.

The optimal design results in the following design variables $o1=(3.000, 0.500, 0.500)$. This design point and a second design point where more uncertainty is observed in the region of interest are added to the DoE used for fitting the metamodel. In this way, the metamodel accuracy is improved in that regions where the optimal is expected and the most error is observed. This results

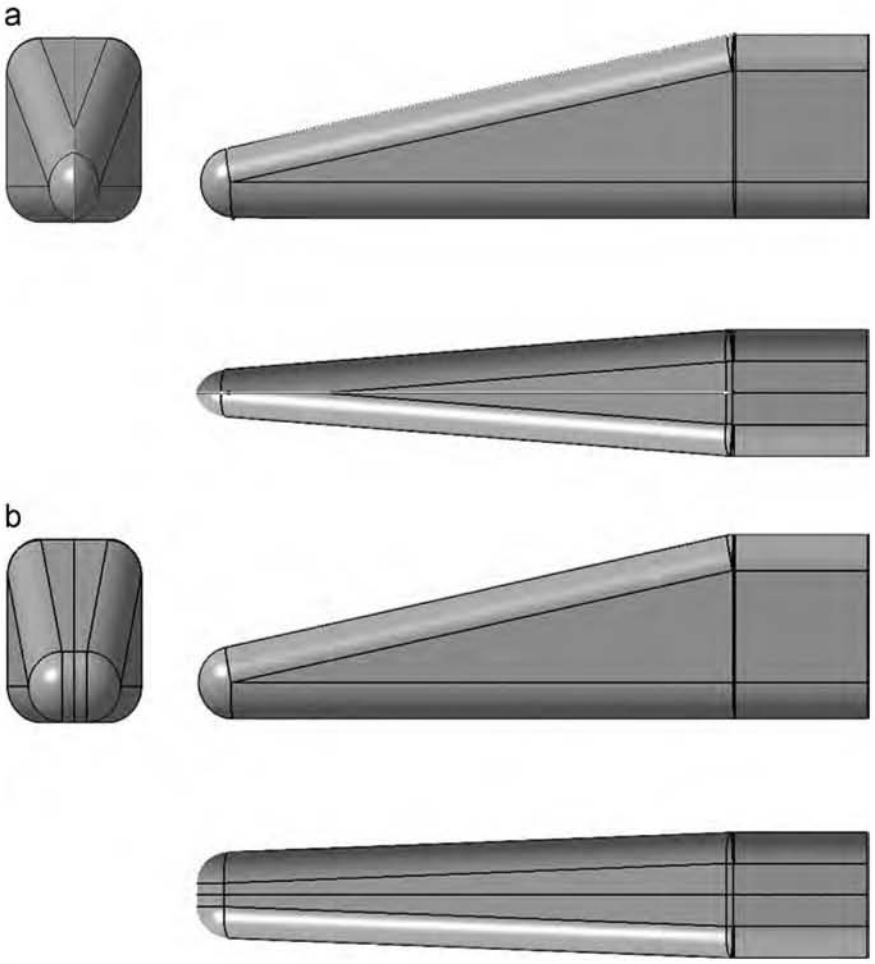

Fig. 4. Optimal shapes for (a) minimum drag coefficient and (b) minimum pressure gradient. The values of the design variables are given in Table 3. (a) *o2* and (b) *optimal*.

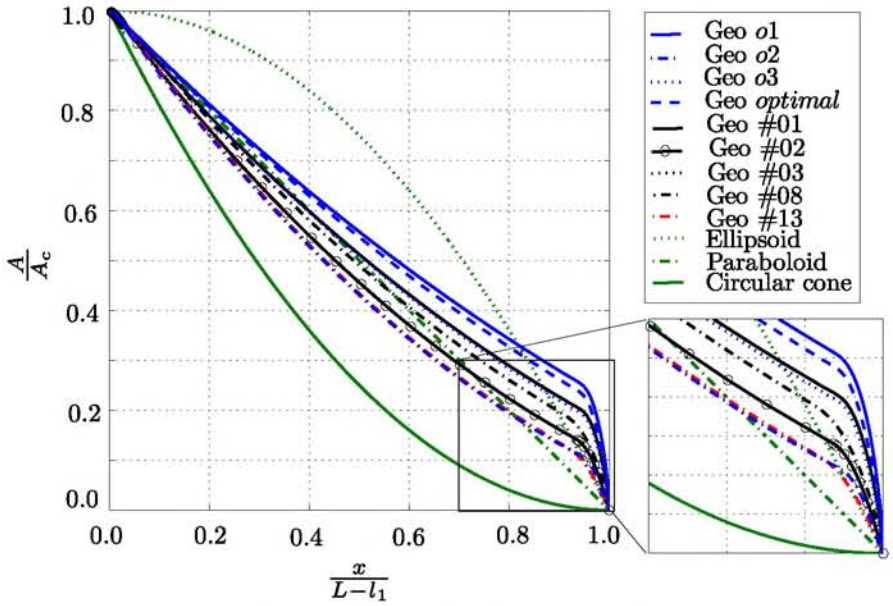

Fig. 5. Cross-sectional area distribution for some representative geometries included in the initial DoE (see Table 1) and obtained during the optimization process (Table 3).

into a new metamodel which is more accurate than the original one. Successive iterations let us increment the quality of the metamodel and thus approximate to the actual optimal. The final optimal is *optimal*=(3.000, 0.500, 0.750). This corresponds to the largest nose length, the bluntest nose shape and the minimum cross-sectional area. After including this design point in the metamodel training, the next iteration converges to the same optimal design, what let us confirm that this is the global optimum. The extra points apart from the ones included in the initial DoE are summarized in Table 3. The best design from the initial data set is also included in the table. It is interesting to remark that the use of metamodels makes possible to reduce the total number of solver calls required during the optimization process. Indeed, this number is 19 in our case (15 from the initial DoE and 4 extra simulations to find the optimal design), while if no surrogate-based optimization is considered, the number would have been the population size (75) times the number of generations required to find the optimum (up to 300). Thus, the benefit of using metamodels is evident.

The tendency in the successive iterations shows that the optimal candidates present the largest nose length, as this is the most important parameter in the maximum pressure gradient. The first optimal candidate $o1$ introduces the maximum bluntness, but the effect of the radius R_1 is still not clear. Therefore, the design $o2$ is included in the data set to increase the information about both effects. The following points show that the optimal candidate converges to the bluntest design and the smallest cross-sectional area. It is interesting to point out that the optimal design for reducing the aerodynamic drag was also obtained during the optimization process. This case corresponds to design $o2$, which is the largest and sharpest nose. The comparison of these two optimal designs is presented in Fig. 4.

A comparison of the geometrical characteristics of these designs is presented in Fig. 5, where the cross-sectional distribution is plotted for some representative geometries. Each geometry is normalized by its respective coach cross-sectional area A_c, *i.e.* the area of the train body and by its nose length L. To complete it, distributions of an ellipsoid, a paraboloid and a conic nose are also plotted. The paraboloid of revolution is considered as the optimal geometry, as it involves a constant rate of change of cross-sectional area. However, Iida et al. (1996) propose an optimal nose shape which has a blunter front end and a slower increase of the cross-sectional area in the middle section of the nose. Ku et al. (2010) confirm this conclusion, and here it is also observed the same behavior. This figure is used to compare the optimal candidates with the geometries from the initial DoE. All the geometries are blunter than the paraboloid of revolution. A zoom of the rate of change at the nose tip is used to stress these differences.

We use the term 'calm' as Torii refers to a nose shape whose cross-sectional area increases slowly. In Fig. 5 it is observed that all the geometries have the same behavior in the middle section, but the differences are observed at the nose tip area distribution. Nevertheless, the optimal design obtained in the optimization has a slightly calmer profile at the middle section, becoming the rate of change of cross-sectional area constant. This policy is effective for not only the reduction of micro-pressure wave at the tunnel, but also the reduction of noise (Torii and Ito, 2000). At the nose tip, the optimal nose and noses corresponding to geometry #01 and $o1$ are the bluntest. The different response of each design is due to the cross-sectional area, being the smallest cross-sectional area the relative to the optimal one. This figure is very useful to compare geometries #02 and #03. It is indicated in Table 1 that geometry #03 is shorter than #02. However, this geometry is better in terms of maximum pressure gradient. Comparing the area distribution of each design, the former is blunter than the latter. Effectively, the value of l_2 is lower for #03, as it can be seen in Table 1.

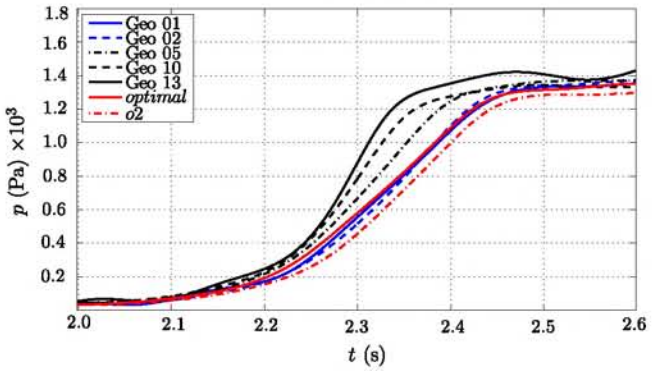

Fig. 6. Compression wave pressure profile (in kPa) for some representative geometries included in the initial DoE and obtained during the optimization process.

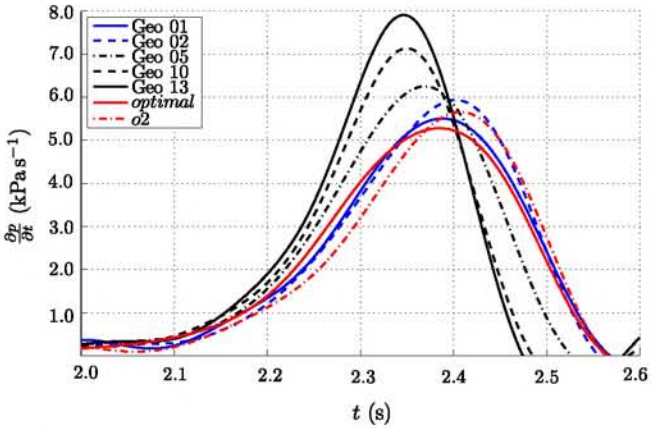

Fig. 7. Compression wave pressure gradient $\partial p/\partial t$ (in kPa s^{-1}) for some representative geometries included in the initial DoE and obtained during the optimization process.

The design $o2$ is the one that introduces a minimum aerodynamic drag. This design is compared with the optimum in terms of maximum pressure gradient (called *optimal*) in the Fig. 5. The difference of the cross-sectional area distribution is evident, showing that $o2$ has a stronger slope at the middle and last section of the nose.

The pressure rise observed at the compression wave generated at the entry of the train and the pressure gradient are plotted in Figs. 6 and 7 respectively. As it was explained before, the pressure rise is almost the same for all the cases, as the blockage ratio varies within a small range of variation. The slope of this curve increases as the length of the train nose is larger. It is observed that the pressure starts increasing before for the blunter noses, but the slope is kept lower than for sharper noses. If the geometries called *optimal* and $o2$ are compared, the former is the bluntest and the corresponding curve starts before than the curve of $o2$ does. However, at the middle section of the pressure rise, the slope is slightly lower than the one belonging to $o2$. This situation is evidenced in Fig. 7, where the gradient of the pressure curve is plotted.

3.3. Aerodynamic aspects

The pressure distribution at the train surface and all along the tunnel walls are represented in Fig. 8. Fig. 8(a) and (b) corresponds to the best and the worst nose of the initial DoE in terms of maximum pressure gradient. It is well known that the peak of the

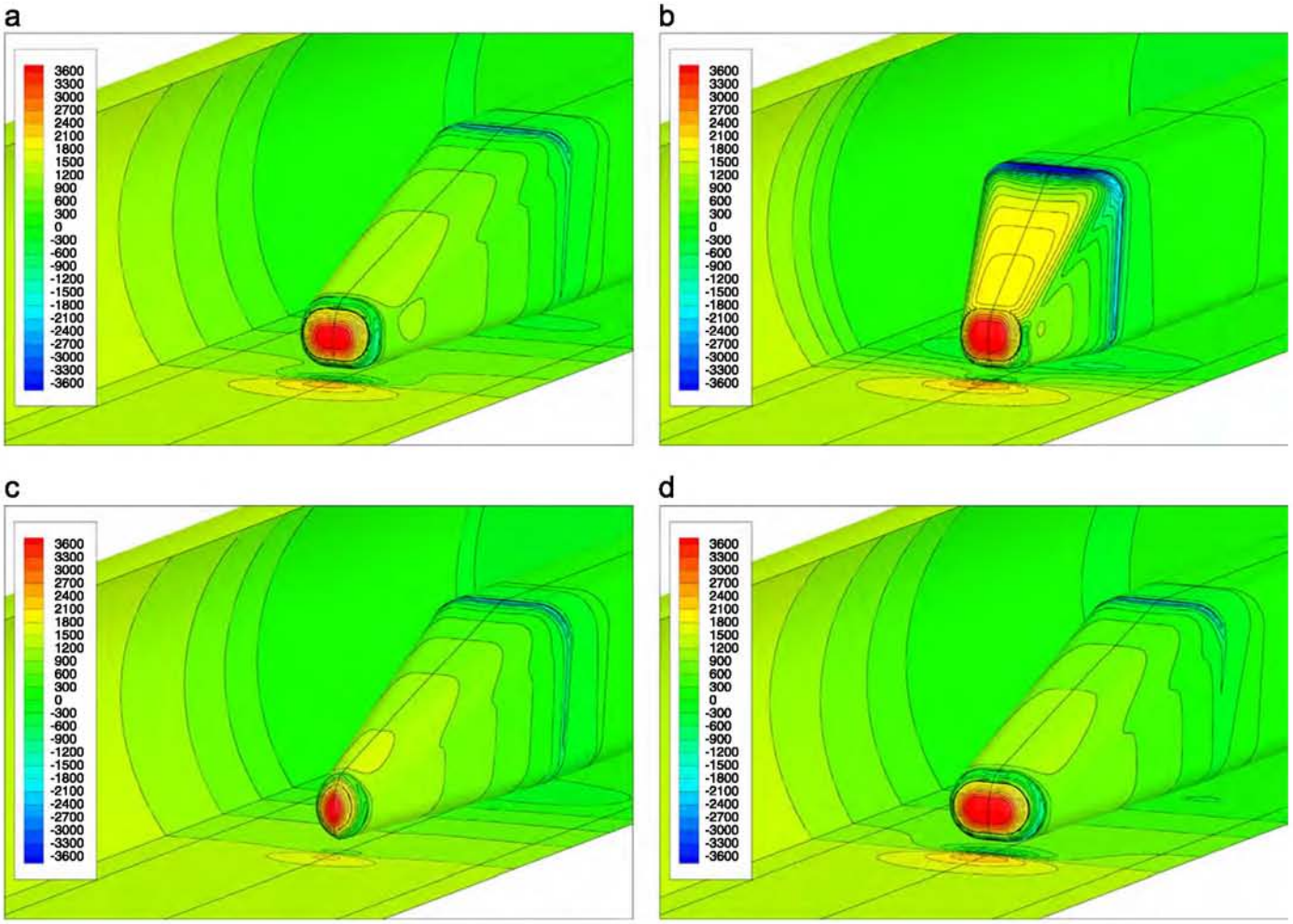

Fig. 8. Pressure fields at the train surface for the most characteristic trains. Pressure is given in Pa. (a) Geo #01, (b) Geo #13, (c) *o2* and (d) *optimal*.

pressure gradient increases with the design variable l_1 (reduction of the slenderness ratio or reduction of the nose length). When the slenderness ratio is decreased, a stronger recirculation region is generated, which increases the effective blockage ratio. This is put in evidence in the case of geometry #13. This geometry is one of the shortest noses and presents a large cross-sectional area. Furthermore, the design variable l_2 is 0.857 m, which is among the highest in our designs. Thus, the flow detachment is observed at the end of the train head, what is presented in Fig. 8. Fig. 8 (c) and (d) compares the optimal geometry for each objective function. Fig. 8(c) corresponds to the minimum aerodynamic drag, while Fig. 8(d) is the geometry with the minimum pressure gradient. Differences of the pressure distribution are observed at the nose tip, where a blunter nose (Fig. 8(d)) provokes a large area of high pressure, and so a large aerodynamic drag. However, the pressure distribution at the side face of the train nose is more uniform for Fig. 8(d) than (c), what might explain the lower maximum pressure gradient.

The compression wave and the pressure gradient generated by this pressure wave are represented in Fig. 9 for the same four cases. These figures permit to observe the intensity of the pressure gradient for the geometry #13 and the shortest noses. The formation of the pressure wave is indicated in Fig. 10. Three instants of time are considered, and the evolution in time of the compression wave generated at the entry of the tunnel is compared for geometry #13 and the geometry called *optimal*, see Table 3.

3.4. Metamodel and global sensitivity analysis

The fact that we are using a surrogate model of the more accurate CFD simulations let us obtain a good approximation of the global behavior of the design space. A three-dimensional representation of the design space is included in Fig. 11. The design variables are normalized as

$$x_i^* = \frac{x_i - x_{i_{\min}}}{x_{i_{\max}} - x_{i_{\min}}}, \quad i = 1 \ldots 3. \tag{4}$$

The design points of the initial DoE and the extra points are plotted as well. The colorbar refers to the maximum pressure gradient. A good accuracy of the metamodel is observed in the training points. It is important to remark that the RBF metamodel does not interpolate but approximate so that the numerical error or noise is not captured or, at least, limited.

As the most important design variable is the nose length, six two-dimensional slices are represented in Fig. 12. In these slices, we can see that for a constant nose length, the influence of the design variable l_2 is more relevant than R_1 one. However, as the slenderness ratio decreases, R_1 gets a more representative influence.

When the number of design variables involved in the construction of the metamodel increases, the number of simulations required for its training rises exponentially. To evaluate the importance of the variables, sensitivity computation is commonly used. The ANOVA test (Ekstrom, 2005) is used for this purpose,

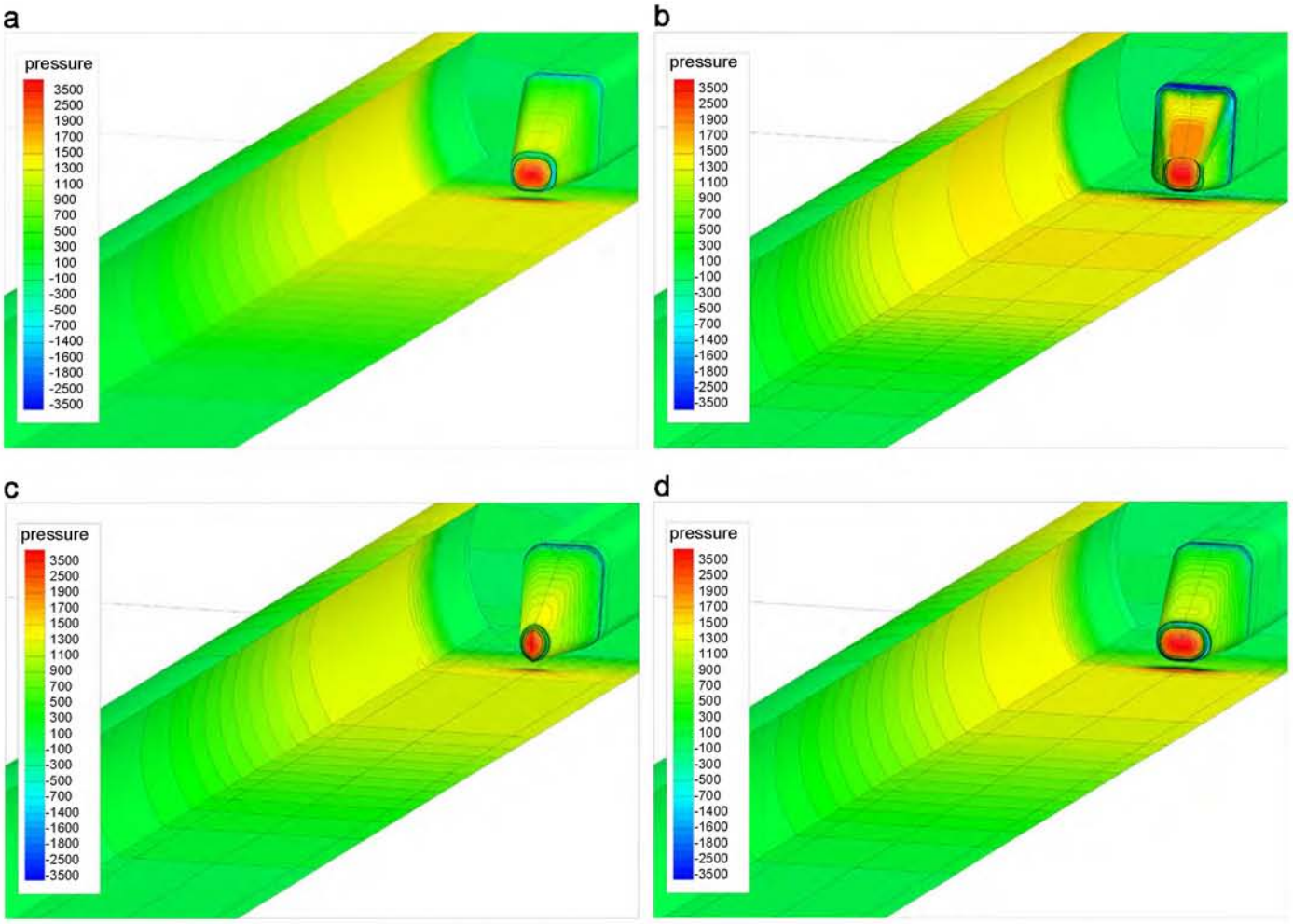

Fig. 9. Pressure fields at the train surface and at the tunnel walls for the most characteristic trains. Pressure is given in Pa. (a) Geo #01, (b) Geo #13, (c) *o2* and (d) *optimal*.

and Sobol indices are the method selected to perform the ANOVA test. This technique is used here not to reduce the curse of dimensionality but to compute which is the effect of each variable. First order sensitivity measures the main effect contribution of each input variable on the output variance, and so on the output response. The sensitivity indices confirm that the main effect corresponds to the design variable l_1, with a 90%, while the effects of l_2 and R_1 are about a 7% and a 3% respectively. These values are obtained after several runs, using a sample size of 2000 points for the Monte Carlo integration. More information about the estimation of the Sobol indices is given in Ekstrom (2005).

3.5. Parametrical analysis of the design variables

3.5.1. Effect of the nose length

Fig. 13 represents the drag coefficient as a function of the nose length (l_1). All the geometrical information about each design was included in Table 1. As l_1 increases, the length of the nose decreases and the drag coefficient in general terms increases. The slenderness ratio decreases because the train width is kept constant. The shape of the nose, in particular the bluntness but also the front area of the nose, do also affect the drag force. Geometry #4 has the minimal C_D among the first fifteen geometries. Squared dots refer to the extra points added during the online optimization. The variation between the optimal C_D case (the largest and sharpest nose) and the optimal $\partial p/\partial t_{\max}$ is about a 24% of the former.

The tendency observed for the maximum pressure gradient is more evident than for the drag coefficient, Fig. 14. The effect of the nose length is more relevant in this case, and it is clear that an increase in the nose length (lower l_1) means a decrease of $\partial p/\partial t_{\max}$. This behavior vanishes for very short nose lengths. When the slenderness ratio is around 2 (for a train width of 3 m, the nose length is about 6 m, so l_1 is 9 m), the influence of the nose length is buffered by the nose shape. When the maximum nose length is considered, there are not big differences between the geometries, and the effect of the bluntness and the blockage ratio is not so evident. Nevertheless, in this figure are compared geometries with very large differences of the nose length, so the maximum pressure gradient is very different as well. Therefore, the possible differences between geometries of the same nose length are attenuated within this range.

3.5.2. Effect of the bluntness of the nose

To visualize the effect of the bluntness of the nose in Fig. 15, only the geometries with the $l_1 = 3.000$ m are considered. As it was indicated previously, a larger value of l_2 produces a lower drag coefficient, as the nose is sharper and more aerodynamic. For the same l_2, a reduction in the cross-sectional area obviously induces a lower drag force. The effect of reducing the cross-sectional area to minimize the drag coefficient is higher than the effect of reducing the bluntness of the nose. If a slenderness angle θ is defined as

$$\tan\theta = \frac{l_2}{L - l_1} \tag{5}$$

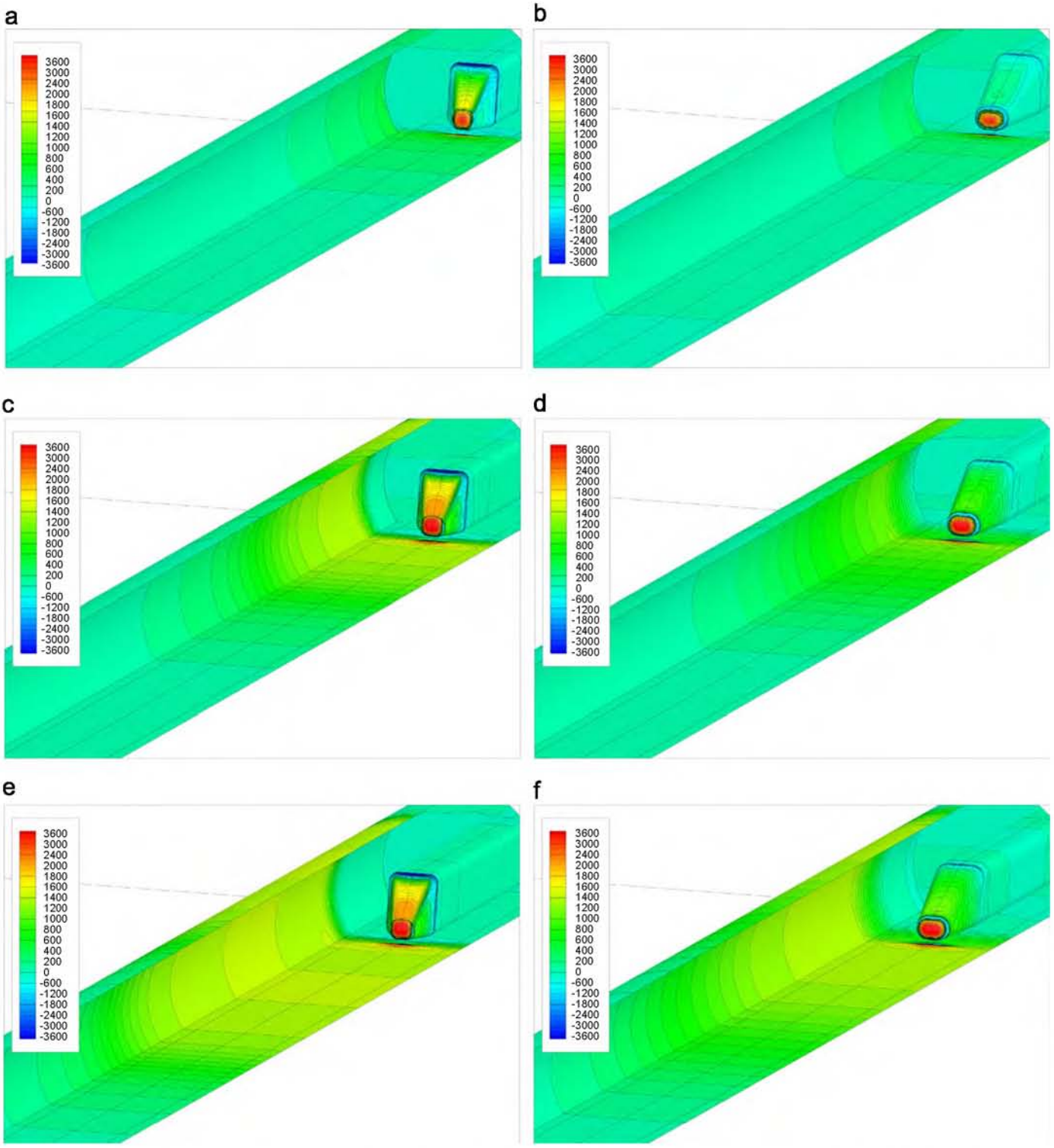

Fig. 10. Time evolution of the compression wave generated when the train enters the tunnel. Pressure is given in Pa. The figures in the left side correspond to the geometry #13 and the figures in the right side to the *optimal* one. (a) $t = 0.0$ s, (b) $t = 0.0$ s, (c) $t = 0.2$ s, (d) $t = 0.2$ s. (e) $t = 0.4$ s and (f) $t = 0.4$ s.

where L is the total length of the train head (15 m) (see Fig. 2), a reduction of the 50% of l_2 is translated into a reduction of the 50% of θ but just an absolute reduction of 0.04 rad, and the decrease in the drag coefficient is about a 19%. Meanwhile, just a reduction of the 3% of the cross-sectional area leads to a decrease of the 6% of the drag coefficient. These conclusions need to be taken with caution, as the values of the θ are very small. For this, if the nose length is very large, the bluntness effect on the drag coefficient is balanced to the cross-sectional area reduction.

In the same Fig. 15, the effect of l_2 on the maximum pressure gradient is also represented. Again there are not big differences between changing the bluntness of the nose and reducing the frontal area, but in percentage, it results more efficient to reduce slightly the cross-sectional area than designing a blunter nose. A

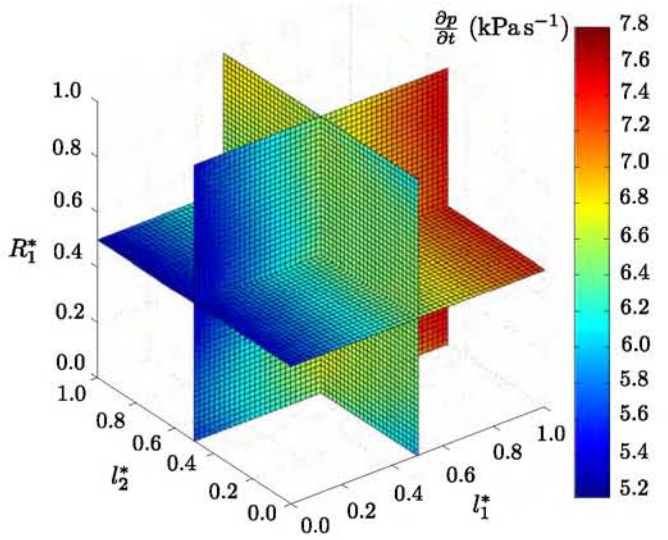

Fig. 11. Three-dimensional representation of the response of the metamodel used for running the single-objective optimization problem. The values of the maximum pressure gradient all over the design space are indicated in color, according to the values of the colorbar. The design variables are normalized according to Eq. (4). (For interpretation of the references to color in this figure legend, the reader is referred to the web version of this paper.)

reduction of 50% of θ gives almost the same decrease of the maximum pressure gradient than a reduction of 3% of the cross-sectional area. Nevertheless, again it is important to keep in mind that the absolute value of θ is very low for large nose lengths, what provokes a large relative change for small absolute modifications.

3.5.3. *Effect of the blockage ratio*

The effect of the blockage ratio is directly related to the effect of the cross-sectional area. In Fig. 15 it is observed that, for the same l_1 and l_2, a reduction of the train section leads to a decrease of both the drag and the maximum pressure gradient. The influence of the cross-sectional area is more important for the drag than for the maximum pressure gradient, where the nose length clearly plays the key role.

3.6. *Estimation of coefficient k*

In Matsuo et al. (1997) a formula of the maximum pressure gradient as a function of the pressure rise and the nose shape is proposed. This equation is

$$\left(\frac{\partial \Delta p}{\partial t}\right)_{comp,max} = \frac{v}{\pi k d_t}\Delta p \tag{6}$$

where v is the train velocity, d_t the equivalent diameter of the tunnel, Δp the pressure rise and k a coefficient that partially includes the nose geometry effect, as it is indicated in Bellenoue et al. (2002). The influence of the nose shape has been evidenced in our results, where the nose length is pointed out as the most critical design variable for the reduction of the maximum pressure gradient, but not the only one. As Δp is a function of the blockage ratio (Eq. (3)), we assume that the effect of R_1 is already included in this term. For this, the objective here is to give an estimation of this coefficient as a function of l_1 and l_2. These two design variables capture the train nose features related to the separation effect. Indeed, Sakuma et al. (2013) observed that a train entering with a separation makes the pressure rise larger than predicted in Eq. (3). Flow separation is clearly related to the nose length and slenderness. Thus, the separation effect is included in the coefficient k. Since lengthening the train nose decreases the amplitude of the pressure gradient, k will increase as we consider larger nose lengths. The values of k for our geometries are presented in the Tables 1 and 3. Our equivalent diameter d_t is 8.956 m, and the train velocity is 69.44 m s^{-1} (250 km h^{-1}). In Bellenoue et al. (2002) and Matsuo et al. (1997), Δp is defined by the pressure at the end of the rapid increase phase, excluding the slow pressure increase due to viscous effects between train and tunnel walls. In our case, Δp is computed using an interval of time Δt_2 at which the viscous-effects pressure increase is partially observed. The reason of doing so is that we are performing a turbulent unsteady simulation and we need this interval to give a good estimation of the pressure amplitude. The consequence is that our pressure amplitude Δp is slightly larger than the corresponding pressure rise introduced by Matsuo although, as it can be seen in Fig. 6, the difference cannot be so relevant.

Our results confirm the tendency aforementioned, with an increase of k as the nose is larger. Our values are slightly larger than the given by Matsuo or Bellenoue (0.33 for a 4 m nose length and 0.37 for 6.75 m). One reason might be the different nose shapes considered in each case. The influence of the bluntness on the maximum pressure gradient provokes that if the nose is sharper, the maximum pressure gradient will be larger and so k will be lower. Moreover, the small differences between the pressure rise calculation would lead to a lower value of k if the pressure rise is slightly lower for the same maximum pressure gradient. Nevertheless, we consider that these explanations do not totally explain such discrepancies.

To approximate the actual value of k as a function of l_1 and l_2 we use a RBF network. The fifteen cases of the initial DoE are used to fit the metamodel coefficients. The other four points are used to check the accuracy of the model. The spread is (1.4, 1.8) and the centers coincide with the data points. λ is set to 1.7×10^{-5}. GCV is used to determine the weights of the RBF network. The final value of GCV is 2.7×10^{-4}.

The metamodel is plotted in Fig. 16. The dots refer to the data points used for fitting the metamodel. Only seventeen designs are identified in the figure because the projection of some of them in this two-dimensional representation hides the rest. A good approximation of the data points is observed in the figure. The prediction error computed from the testing points is 3%. The figure shows that the main effect is the nose length, and that the design variable l_2 effect is not so critical. This confirms what is presented in Bellenoue et al. (2002). Nevertheless, if a most accurate prediction is expected, it is necessary to consider the bluntness as well. Our results indicate that the difference is about a 7% for noses of the same nose length and different nose shapes. The influence of R_1 is negligible in the range of values that we imposed. This conclusion is in good agreement with our first assumption, as the blockage ratio is included in the pressure rise in Eq. (6).

4. Multi-objective optimization

It has been indicated that a blunter nose results into a lower maximum pressure gradient, while this geometrical characteristic becomes a drawback when the aerodynamic drag is the objective function to be minimized. Therefore, it is observed that there are objectives in conflict in the multi-objective optimization problem of designing a high-speed train nose. The metamodel presented in Section 3.2 refers to the first objective function. If a second metamodel is constructed to approximate the drag coefficient of the previous geometries, it is possible to run a surrogate-based multi-objective optimization process. The purpose is to obtain a Pareto front that contains a set of optima regarding to this two objectives. This problem is solved using MATLAB® function `gamultiobj`. The Pareto front population fraction is 0.35 and

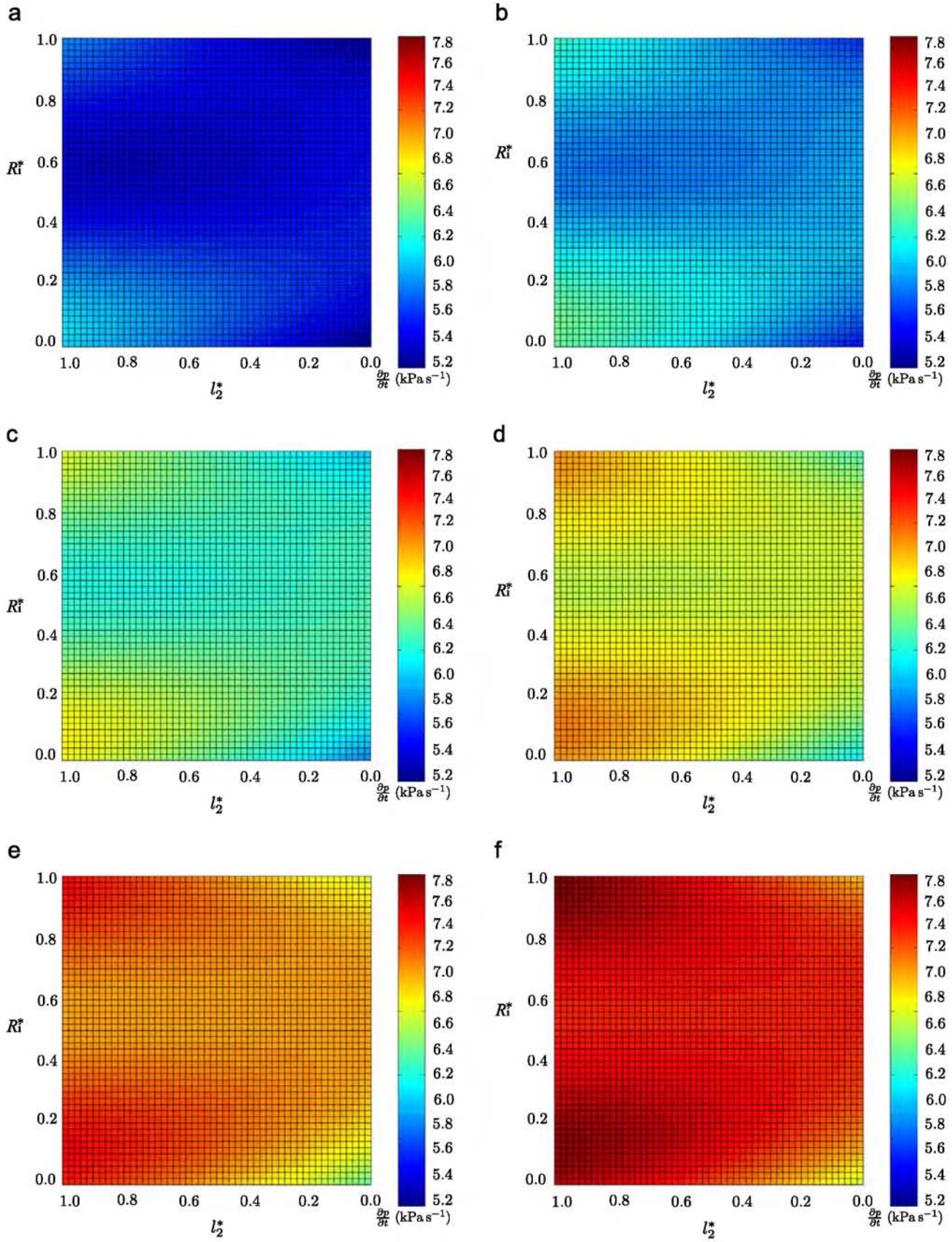

Fig. 12. Two-dimensional visualization of the response of the metamodel used for running the single-objective optimization problem. The slices correspond to constant values of l_1. (a) $l_1 = 3.0$ m, (b) $l_1 = 4.8$ m, (c) $l_1 = 6.6$ m, (d) $l_1 = 8.4$ m, (e) $l_1 = 10.2$ m and (f) $l_1 = 12.0$ m.

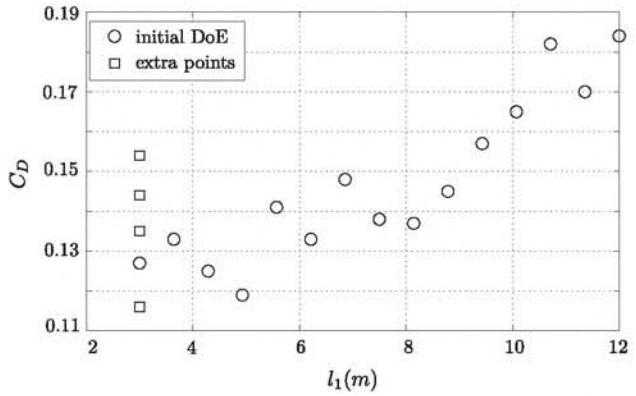

Fig. 13. Effect of the nose length in the aerodynamic drag. Circular dots refer to the geometries of the initial DoE. Squared dots correspond to the extra points indicated in Table 3.

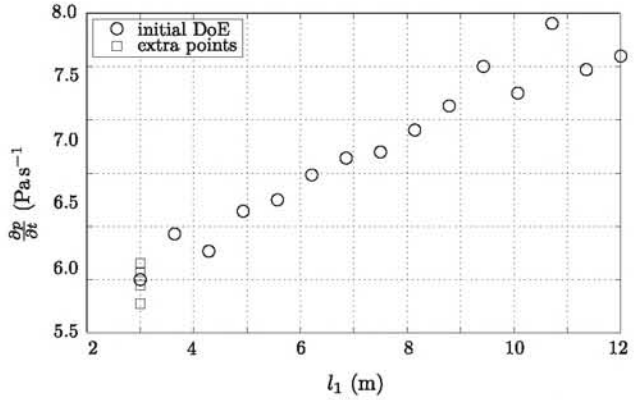

Fig. 14. Effect of the nose length in the maximum pressure gradient. Circular dots refer to the geometries of the initial DoE. Squared-dots correspond to the extra points indicated in Table 3.

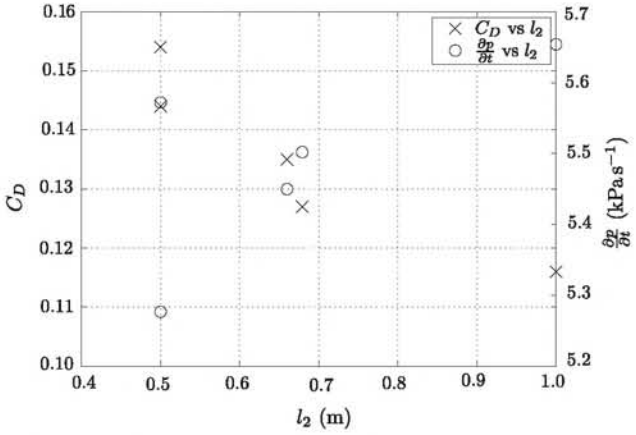

Fig. 15. Effect of the nose bluntness or l_2 in the aerodynamic drag an the maximum pressure gradient.

the distance measure fraction is `distancecrowding`, implemented in MATLAB®. The population size is increased to 100, so that we can avoid a disconnected Pareto front. The rest of the parameters are set equal to the single-objective optimization.

The optimization is stopped when the average change in the spread of the Pareto front is less than 10^{-4}. The number of generations is 130 and the number of points in the Pareto front is 32. The resulting Pareto front is given in Fig. 17. The average Pareto distance is 0.567 and the average Pareto spread is 0.34. A more complete description of the meaning of these parameters is included in MAT (2013). It is clearly observed that the two

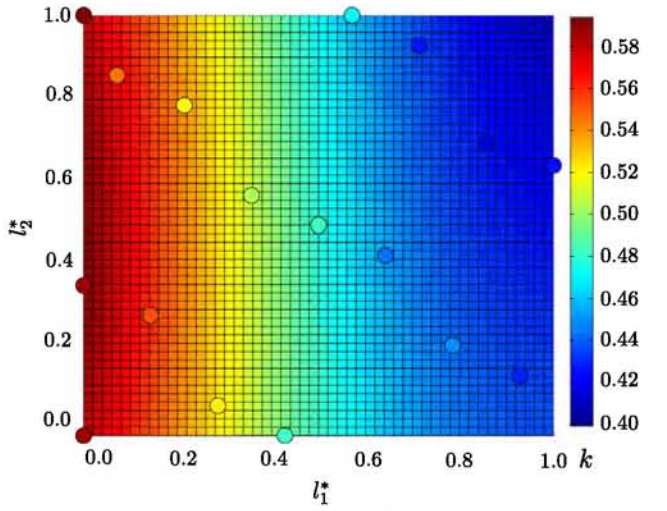

Fig. 16. Values of the coefficient k, from Eq. (6), obtained by the metamodel are represented in the design space. A two-dimensional (l_1^*, l_2^*) visualization of the design space is considered. Circular dots refer to the train noses included in the initial DoE, see Table 1, and the optimal design to minimize the drag coefficient (namely O_2) and to minimize the maximum pressure gradient (*optimal*), see Table 3.

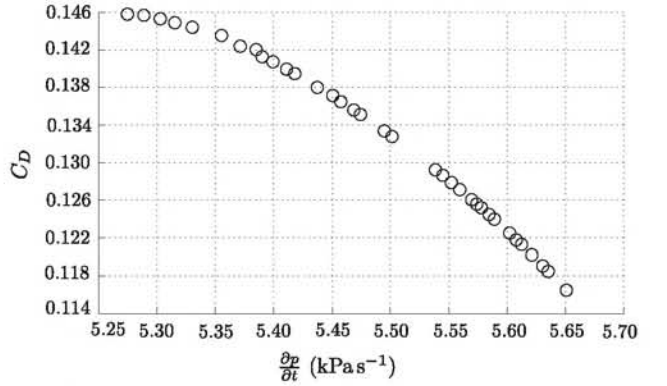

Fig. 17. Pareto front resulting of the multi-objective optimization problem, minimizing the maximum pressure gradient and the drag coefficient.

objectives are in conflict. A reduction of the drag coefficient leads to a higher maximum pressure gradient, while geometries that minimize the maximum pressure gradient are blunter and introduce a larger drag. The endpoints of the Pareto front correspond to the two optimal points obtained in the single-objective optimization. The Pareto front given in Suzuki and Nakade (2013) is similar to the one obtained in this paper. The different features of the optimal nose shape for minimizing the aerodynamic drag and the pressure distribution along the nose are also observed in our study, as it was demonstrated in Fig. 4.

5. Summary

We have presented in this paper a large set of three-dimensional, turbulent, compressible, unsteady simulations of realistic train models. The baseline of all the train models is known as 'generic train', but we introduced an extra design variable to obtain a more complete design space. The resulting geometry parameterization let us to study the main parameters affecting both the compression wave generated at the entry of the train and the aerodynamic drag on the train. These parameters are the nose length, the nose shape (bluntness, A-pillar roundness, etc.) and the blockage ratio. Our simulations are in good agreement with the

results and conclusions of different references. These results confirm the key role of the nose length as the most representative geometrical parameter for the reduction of the maximum pressure gradient of the nose of a high-speed train. Nevertheless, the influence of other design variables, as l_2, has been studied.

These previous analyses are used to outline a single-objective optimization problem, where the objective function is the minimization of the maximum pressure gradient of the compression wave. Among the different optimization methods available to solve this problem, we have chosen the genetic algorithms (GA). The necessity of a large number of evaluations of the objective function to determine which is the optimal design drives to the construction of a metamodel. This metamodel or surrogate model substitutes the more accurate numerical simulation, but reduces dramatically the computational cost of the optimization process. A RBF network has been considered in this case, and its accuracy and prediction capability have been indicated. The resulting optimal design confirms the tendency indicated in different references, where a large and blunt nose reduces the maximum pressure gradient.

However, this geometrical design provokes an increase of the aerodynamic drag, which needs to be considered as the train will also travel in open air. For this, a multi-objective optimization problem has been proposed, and a Pareto front has been obtained as the solution. This Pareto front contains a set of optimal solutions, whose endpoints correspond to the optimal design for each single objective function.

To complete the study, a new metamodel has been constructed to approximate the relationship of the pressure rise of the compression wave, the maximum pressure gradient and the nose shape.

Acknowledgments

This work is financed by Ministerio de Ciencia e Investigación (Eng. Ministry of Science and Technology) under contract TRA-2010-20582, included in the VI Plan Nacional de I+D+i 2008–2011. It is also a part of the research project included in Subprograma INNPACTO, from Ministerio de Ciencia e Innovación.

References

Auvity, B., Bellenoue, M., Kageyama, T., 2001. Experimental study of the unsteady aerodynamic field outside a tunnel during a train entry. Exp. Fluids 30, 221–228.

Auvity, B., Bellenoue, M., Kageyama, T., 2002. Structure and evolution of the airflow generated by a slender body entry near a tube. Eur. J. Mech. B/Fluids 21, 157–170.

Baron, A., Molteni, P., Vigevano, L., 2006. High-speed trains: prediction of micro-pressure wave radiation from tunnel portals. J. Sound Vib. 296, 59–72.

Baron, A., Mossi, M., Sibilla, S., 2001. The alleviation of the aerodynamic drag and wave effects of high-speed trains in very long tunnels. J. Wind Eng. Ind. Aerodyn. 89 (5), 365–401.

Bellenoue, M., Moriniere, V., Kageyama, T., 2002. Experimental 3d simulation of the compression wave, due to train-tunnel entry. J. Fluids Struct. 16 (5), 581–595.

Ekstrom, P.-A., 2005. EIKOS: A Simulation Toolbox for Sensitivity Analysis in MATLAB. FACILIA AB.

Gawthorpe, R.G., Pope, C.W., Green, R.H., 1979. Analysis of train drag in various configurations of a long tunnel. In: 3rd International Conference on the Aerodynamics and Ventilation of Vehicle Tunnels Cranfield, UK.

Goldberg, D.E., 1989. Genetic Algorithms in Search, Optimization and Machine Learning, 2nd edition Addison-Wesley Publishing Company, Reading Menlo Park, California.

Hara, T., 1961. Aerodynamic force acting on a high speed train at tunnel entrance. In: Bulletin of JSME. Japanese Society of Mechanical Engineers.

Heine, D., Ehrenfried, K., 2012. Experimental study of the compression-wave generation due to train-tunnel entry. In: Proceedings of the First International Conference on Railway Technology: Research, Development and Maintenance.

Holland, J.H., 1975. Adaptation in Natural and Artificial Systems, 1st edition The University of Michigan Press, Michigan.

Howe, M.S., 2005. On the role of separation in compression wave generation by a train entering a tunnel hood with a window. IMA J. Appl. Math. 70 (3), 400–418.

Howe, M.S., 2007. The genetically optimized tunnel entrance hood. J. Fluids Struct. 23, 1231–1250.

Howe, M.S., Iida, M., Fukuda, T., Maeda, T., 2000. Theoretical and experimental investigation of the compression wave generated by a train entering a tunnel with a flared portal. J. Fluid Mech. 425, 111–132.

Howe, M.S., Iida, M., Maeda, T., Sakuma, Y., 2006. Rapid calculation of the compression wave generated by a train entering a tunnel with a vented hood. J. Sound Vib. 297 (1), 267–292.

Husslage, B., Rennen, G., van Dam, E.R., den Hertog, D., 2006. Space-filling latin hypercube designs for computer experiments. Discussion Report 2006-18, Tilburg University.

Iida, M., Matsumura, T., Nakatani, K., Fukuda, T., Maeda, T., 1996. Optimum nose shape for reducing tunnel sonic boom. In: IMECHE Conference Transactions, Mechanical Engineering Publications, vol. 8, pp. 271–282.

Jakubek, D., Wagner, C., 2012. Shape optimization of train head cars using adjoint-based computational fluid dynamics. In: Pombo, J. (Ed.), Proceedings of the First International Conference on Railway Technology: Research, Development and Maintenance, vol. 1. Las Palmas de Gran Canaria, Spain.

Kikuchi, K., Iida, M., Fukuda, T., 2011. Optimization of train nose shape for reducing micro-pressure wave radiated from tunnel exit. J. Low Freq. Noise, Vib. Active Control 30 (1), 1–19.

Krajnovic, S., 2009. Optimization of aerodynamic properties of high-speed trains with cfd and response surface models. In: The Aerodynamics of Heavy Vehicles II: Trucks, Buses, and Trains, Lecture Notes in Applied and Computational Mechanics, vol. 41. Springer Berlin Heidelberg, pp. 197–211.

Ku, Y.-C., Rho, J.-H., Yun, S.-H., Kwak, M.-H., Kim, K.-H., Kwon, H.-B., Lee, D.-H., 2010. Optimal cross-sectional area distribution of a high-speed train nose to minimize the tunnel micro-pressure wave. Struct. Multidiscip. Optim. 42, 965–976.

Kwon, H.-B., Jang, K.-H., Kim, Y.-S., Yee, K.-J., Lee, D.-H., 2001. Nose shape optimization of high-speed train for minimization of tunnel sonic boom. JSME Int. J. Ser. C 44 (3), 890–899.

Lee, J., Kim, J., 2008. Approximate optimization of high-speed train nose shape for reducing micropressure wave. Struct. Multidiscip. Optim. 35 (1), 79–87.

MAT, 2013. Optimization Toolbox. User's Guide R2013b. The MathWorks, Inc.

Maeda, T., Matsumura, T., Iida, M., Nakatani, K., Uchida, K., 1993. Effect of shape of train nose on compression wave generated by train entering a tunnel. In: The International Conference on Speedup Technology for Railway and Maglev Vehicles.

Matsuo, K., Aoki, T., Mashimo, S., Nakatsu, E., 1997. Entry compression wave generated by a high-speed train entering a tunnel. In: 9th International Conference on the Aerodynamics and Ventilation of Vehicle Tunnels Aosta, Italy. BHR Group Conference.

Miyachi, T., Ozawa, S., Arai, T., 2012. Theoretical study on the compression wave produced by a train entering a tunnel. Application of acoustic theory to the case of high blockage ratio problem. J. Jpn. Soc. Fluid Mech. 31, 45–59.

N'Kaoua, J., Pope, C.W., Henson, D.A., 2006. A parametric study into the factors affecting the development and alleviation of micro-pressure waves in railway tunnels. In: 12th International Symposium on Aerodynamics and Ventilation of Vehicle Tunnels, Portoroz, Slovenia, pp. 789–803.

Ogawa, T., Fujii, K., 1997. Numerical investigation of the three-dimensional compressible flows induced by a train moving into a tunnel. Comput. Fl 26 (6), 565–585.

Orr, M.J., 1996. Introduction to Radial Basis Function Networks. Centre for Cognitive Science, University of Edinburgh, UK.

Raghunathan, R.R., Kim, H., Setoguchi, T., 2002. Aerodynamics of high-speed railway train. Prog. Aerosp. Sci. 38, 469–514.

Sakuma, Y., Fukuda, T., Miyachi, T., Ido, A., 2013. Improving the aerodynamic performance of flat-fronted trains on meter-gauge railway lines. Q. Rep. RTRI 54 (4), 222–230.

Schetz, J.A., 2001. Aerodynamics of high-speed trains. Ann. Rev. Fluid Mech. 33, 371–414.

Sima, M., Grappein, E., Weise, M., Paradot, N., Hieke, M., Baker, C., Licciardello, R., and Couturier, M., 2011. Presentation of the eu fp7 aerotrain project and first results. In: 9th World Congress on Railway Research. Challenge G: An Even More Competitive and Cost Efficient Railway Lille, France.

Suzuki, M., Nakade, K., 2013. Multi-objective design optimization of high-speed train nose. J. Mech. Syst. Transp. Logist. 6, 54–64.

Torii, A., Ito, J., 2000. Development of the series 700 shinkansen train-set. Jpn. Railw. Eng. 14, 16–18.

Vardy, A.E., 1996. Aerodynamic drag on trains in tunnels. Part 2. Prediction and validation. Proc. Inst. Mech. Eng., Part F: J. Rail Rapid Transit 210 (1), 39–49.

Vardy, A.E., 2008. Generation and alleviation of sonic booms from rail tunnels. Proc. ICE – Eng. Comput. Mech. 161 (3), 107–119.

Vytla, V.V., 2011. Multidisciplinary Optimization Framework for High Speed Train using Robust Hybrid GA-PSO Algo (Ph.D. thesis). Wright State University, Department of Mechanical and Materials Engineering.

Yoon, T., Lee, S., Hwang, J.H., Lee, D.H., 2001. Prediction and validation on the sonic boom by a high-speed train entering a tunnel. J. Sound Vib. 247 (2), 195–211.